Title

Novel Antimycobacterial Compounds Suppress NAD Biogenesis by Targeting a Unique Pocket of NaMN Adenylyltransferase

Journal

ACS Chemical Biology, 14(5)

ISSN

1554-8929

Authors

Osterman, Andrei L
Rodionova, Irina
Li, Xiaoqing
et al.

Publication Date

2019-05-17

DOI

10.1021/acschembio.9b00124

Peer reviewed

Published in final edited form as:

ACS Chem Biol. 2019 May 17; 14(5): 949–958. doi:10.1021/acschembio.9b00124.

Novel antimycobacterial compounds suppress NAD biogenesis by targeting a unique pocket of NaMN adenylyltransferase

Andrei L. Osterman[1], **Irina Rodionova**[1,†], **Xiaoqing Li**[1], **Eduard Sergienko**[2], **Chen-Ting Ma**[2], **Antonino Catanzaro**[3], **Mark E. Pettigrove**[3], **Robert W. Reed**[4,‡], **Rashmi Gupta**[5], **Kyle H. Rohde**[5], **Konstantin V. Korotkov**[4,*], **Leonardo Sorci**[6,*]

[1]Sanford Burnham Prebys Medical Discovery Institute, La Jolla, CA, United States

[2]NCI Designated Cancer Center, Sanford Burnham Prebys Medical Discovery Institute, La Jolla, CA, United States

[3]Department of Medicine, University of California San Diego, La Jolla, CA, United States

[4]Department of Molecular and Cellular Biochemistry, College of Medicine, University of Kentucky, Lexington, KY, United States

[5]Division of Immunity and Pathogenesis, Burnett School of Biomedical Sciences, College of Medicine, University of Central Florida, Orlando, FL, United States

[6]Department of Materials, Environmental Sciences and Urban Planning, Division of Bioinformatics and Biochemistry, Polytechnic University of Marche, Ancona, Italy

Abstract

Conventional treatments to combat the tuberculosis (TB) epidemic are falling short, thus encouraging the search for novel antitubercular drugs acting on unexplored molecular targets. Several whole cell phenotypic screenings have delivered bioactive compounds with potent antitubercular activity. However, their cellular target and mechanism of action remain largely unknown. Further evaluation of these compounds may include their screening in search for known antitubercular drug targets hits. Here, a collection of nearly 1,400 mycobactericidal compounds was screened against *Mycobacterium tuberculosis* NaMN adenylyltransferase (*Mt*NadD), a key enzyme in the biogenesis of NAD cofactor that was recently validated as a new drug target for dormant and active tuberculosis. We found three chemotypes that efficiently inhibit *Mt*NadD at low micromolar range *in vitro*. SAR and cheminformatics studies of commercially available analogs point to a series of benzimidazolium derivatives, here named N2, with bactericidal activity on different mycobacteria, including *M. abscessus*, multidrug resistant *M. tuberculosis,* and dormant *M. smegmatis*. The on-target activity was supported by the increased resistance of a *M. smegmatis* strain overexpressing the target, and by a rapid decline in NAD(H) levels. A co-

*Correspondence to: Leonardo Sorci, l.sorci@staff.univpm.it; Konstantin V. Korotkov, kkorotkov@uky.edu.

†present address: Department of Molecular Biology, Division of Biological Sciences, University of California, San Diego, La Jolla, CA, United States

‡present address: Division of Regulatory Services, College of Agriculture, Food and Environment, University of Kentucky, Lexington, Kentucky, United States

Accession Codes

Atomic coordinates and structure parameters have been deposited in the Protein Data Bank (www.rcsb.org) with accession code 6BUV.

crystal structure of *Mt*NadD with **N2–8** inhibitor reveals that the binding of the inhibitor induced the formation of a new quaternary structure, a dimer-of-dimers where two copies of the inhibitor occupy symmetrical positions in the dimer interface, thus paving the way for the development of a new generation of selective *Mt*NadD bioactive inhibitors. All these results strongly suggest that pharmacological inhibition of *Mt*NadD is an effective strategy to combat dormant and resistant *Mtb* strains.

Graphical Abstract

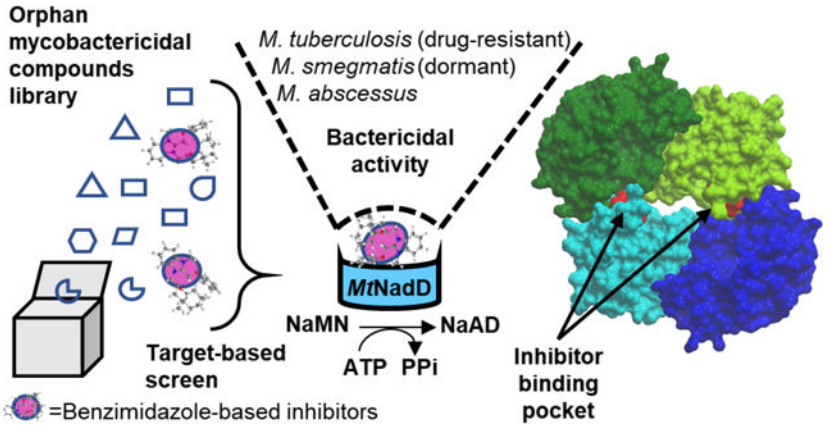

Introduction

Despite extensive prevention and control measures in the last two decades, Tuberculosis yet represents a dramatic health issue with global impact. The World Health Organization (WHO) estimates over ten million active disease cases in 2016 and nearly 1.7 million deaths, 22% of which were among immunocompromised HIV-positive individuals[1]. *Mycobacterium tuberculosis* (*Mtb*), which causes TB, undergoes a metabolic shift in the human host into a dormant state resulting in long-term persistent infection and phenotypic resistance to many otherwise successful drugs[2–4]. Drug susceptible strains can be effectively treated with a 6 to 9-month regimen of multiple antibiotics, but the non-adherence to the therapeutic guidelines on a global level has exacerbated the selection and spreading of resistant strains in the last two decades[5]. Particularly alarming is the increase of multidrug-resistant tuberculosis (MDR-TB), resistant to isoniazid and rifampicin, two of the most powerful TB drugs, and extensively drug resistant (XDR-TB), which are additionally resistant to any fluoroquinolone, and to at least one of the second line drugs (amikacin, capreomycin or kanamycin)[6].

Consensus is growing that novel, much needed antibiotics, should efficiently kill drug-resistant strains and dormant mycobacteria as well as shorten therapy via novel targets[2, 3].

Two novel classes of antibiotics, diarylquinolines and nitroimidazoles, have reached stage III of clinical trials, proving to be effective alone in treating latent tuberculosis (LTB) [7–10]. Bedaquiline (BDQ), the first-in-class compound of diarylquinolines, is the first new drug in decades to be clinically approved for TB treatment. In particular,

due to its unique mechanism of action on mycobacterial ATP synthase, bedaquiline opened a new door for discovering anti-TB/LTB drugs using oxidative phosphorylation as a target system[11]. However, resistance to BDQ has already been observed. Besides the selection of mutations of the *atp*E subunit of target ATP synthase, drug-responsive mechanisms involve activation of dormancy and metabolic remodeling [12, 13]. Notably, alternative ATP production from substrate-level phosphorylation appear to enable transient bacterial survival, as further confirmed by BDQ-enhanced killing of mycobacteria on non-fermentable energy sources[13]. Glycolysis not only produces ATP faster, albeit less efficiently, than oxidative phosphorylation but also supplies metabolic precursors required for macromolecular biosynthesis. Strikingly, glycolytic enzymes are upregulated in BDQ-treated mycobacteria, including lactate dehydrogenase that recycles NADH to NAD[13]. These observations emphasize the significance of targeting other aspects of energy metabolism that are essential for both actively replicating and dormant forms of mycobacteria.

Biogenesis and homeostasis of redox cofactors, most notably of NAD pool (NAD(H) and NADP(H)), is another crucial aspect of respiratory energy metabolism in both, replicating and dormant forms of mycobacteria [14, 15].

NAD(H) is the entry electron donor in respiratory chain and the key oxidant driving the glycolysis. Thus, depletion of NAD(H) pool generates a glycolytic slowdown [16] and a rapid shutdown of electron transfer chain thereby affecting ATP synthesis from both sources.

In this view, NAD starvation, which represents alone a validated strategy to kill mycobacteria recalcitrant to current therapies[17, 18], may potentially show synergy with drugs targeting ATP synthesis such as bedaquiline.

The universally conserved and essential enzymes, NadD, NadE and NadF, which drive the last non-redundant steps of NAD(P) biosynthesis, were implicated by our previous genomics-driven studies as potential drug targets in numerous bacterial pathogens[19–22]. Of these three enzymes, NadD is the most divergent from its human counterparts (NMNAT1–3[23]), offering the opportunity of developing selective small-molecule inhibitors[22, 24–27]. Our recent studies showed that induced degradation of NadD and NadE enzymes in a model system of *M. smegmatis* (*Msm)* led to rapid depletion of the NAD cofactor pool followed by cell death, even under non-replicative conditions[17]. Another group used a similar approach to show that induction of NadE degradation also suppressed acute and chronic *Mtb* infection in mice[18]. These findings provided ultimate validation of NAD metabolism as a target pathway for the development of new antimycobacterial therapies. Structure-function and inhibition studies of the key NAD(P) biosynthetic enzymes [22, 24, 25, 28, 29] including our recently published work on *Mt*NadD[26] support their druggability.

We set out to identify inhibitors of *Mt*NadD through a target-based screen of orphan compounds with mycobactericidal activity. Here, we report the identification as well as the biochemical and biological characterization of several potent inhibitors of NadD with bactericidal activity on mycobacteria, including *M. abscessus*, multidrug-resistant *M. tuberculosis*, as well as a prominent bactericidal effect under non-replicating conditions in *M. smegmatis*. To clarify in atomic detail the mode of action of these compounds and

their structure-activity relationships, we also determined the crystal structure of *Mt*NadD in complex with one of these inhibitors.

RESULTS AND DISCUSSION

Screening of bioactive antimycobacterial compounds affords novel *Mt*NadD inhibitors.

Previous whole cell phenotypic screening has identified potent anti-mycobacterial compounds in a variety of tested conditions on replicating, non-replicating and intracellular forms of *Mtb*. These compounds were selected via several cell-based HTS campaigns as reported in PubChem [30, 31], but their mechanisms and molecular targets remain unknown. We speculated that, given a limited space of potential targets (~200–300 essential genes in *M. tuberculosis*), at least some of these compounds could target the essential enzymes of NAD metabolism. For this reason, a collection of 1389 bioactive compounds, kindly provided by Global Alliance for TB Drug Development (TB Alliance) was tested against the recombinant *M. tuberculosis* NadD enzyme using colorimetric detection assay of released PPi (Figure 1). The primary assays, performed at fixed final concentration of 25 μM for each compound, and at subsaturating concentrations of ATP and NaMN, identified 16 compounds (~1% hit rate) inhibiting more than 30% of enzymatic activity, with three of these demonstrating >50% inhibition. Notably, this hit rate is comparable to our previous structure-based approach on NadD from *Escherichia coli* and *Staphylococcus aureus* [24] which, however, used a more stringent concentration of the inhibitor (100 μM). These primary hits were repurchased from different vendors and their concentration-response profiling yielded 5 compounds with IC_{50} values in the range of 6–22 μM (Supplementary Table 1). The three top-ranked compounds with significant structural diversity, termed here as N1, N2, and N3, were selected for further analysis, including cheminformatics and SAR studies by analogs' testing, cell-based assays, and co-crystallization trials (Figure 1).

SAR for chemotypes N1, N2, and N3.

Before any further investigation on these chemotypes was pursued, we wanted to confirm their bioactivity as originally displayed in whole cell phenotypic assay. For example, we determined a minimal inhibitory concentration of 28 μM of the compound **N2–11** for *M. tuberculosis* H37Rv. This result is consistent with the inhibition value reported in PubChem Bioassay 1626 (MIC of 16 μM). Overall, around 30 analogs of the 3 selected chemotypes were purchased from different vendors and tested *in vitro* against *Mt*NadD (Figure 2 and Tables 1–3). Despite a limited chemical search exploration, 4 analogs show improved *Mt*NadD inhibition relative to their parent compound, with up to 5-fold lower IC_{50} (2.5 μM) for **N1–11** analog, which represents the most potent inhibitor for *Mt*NadD described so far [26].

In class N1, the replacement of a 3-fluoro benzyl group with the more hydrophobic 1-phenylethyl (**N1–11**) or benzyl (**N1–10**) moieties yielded the best improvement. More polar moieties such as five- or six-membered rings with two or more heteroatoms were poorly tolerated (IC_{50} > 50–100 μM), while linear or branched hydrocarbon chains (**N1–6** through **N1–8**), or the smaller cyclopropyl moieties (**N1–9**) were well-tolerated substitutions (15 μM

< IC_{50} < 40 μM), underlying the importance of the hydrophobic character in this inhibitor moiety.

Regarding class N2, is worth mentioning that three analogs were already identified in the primary screening, namely **N2–7**, **N2–9**, and **N2–11**. This class features a benzimidazolium core with a methyl and a 2-isopropyl-5-methylcyclohexyl-containing moiety at each N atom. All N2 tested analogs were active, although they did not significantly improve the parent compound potency. Of the two weaker analogs, compound **N2–2**, replacing a bulky methoxyphenyl or dimethoxyphenyl group in C-1 position of benzimidazole by a methyl group displays a substantially lower inhibitory activity (IC_{50} ~100 μM). The replacement with a bromophenyl (**N2–6**) yields an intermediate IC_{50} of 45 μM, pointing to the importance of the size of this moiety. The remaining analogs of this series, containing a methoxyphenyl group have similar activities compared to the parent compounds (5 μM < IC_{50} < 20 μM) and yield a bland structure-activity profile. The only analog with a slightly improved activity (**N2–1**, IC_{50} of 4.8 μM) has a distinct structure with two symmetric 2-isopropyl-5-methylcyclohexyl-containing moieties. The two **N3** analogs tested in this study demonstrated a marked decrease in activity (Figure 2 and Table 3). We therefore did not follow up this compound in more detail.

At this stage, all tested analogs were selected only based on structural similarity, without any attempts of their rational improvement. Nevertheless, some analogs in series N1 and N2 displayed a moderate to significant improvement of inhibition efficacy, compared with the parent compounds, showing to be amenable to chemical optimization.

Effects of *Mt*NadD inhibitors on mycobacteria cell growth.

Our original hits against *Mt*NadD activity have potent antitubercular activities with reported EC_{50} in the low micromolar range (see results in PubChem for bioassay AID 1626) and reconfirmed by us as shown hereafter. *Mt*NadD IC_{50} values are in the same order of magnitude (Tables 1–3), which is not unexpected since we demonstrated with a protein knock-down system that partial inhibition of *Mt*NadD is sufficient to kill mycobacteria [17]. To direct the choice of compounds for further evaluation, we next assessed their ability to also suppress the growth of *M. smegmatis*. Besides being a convenient nonpathogenic and rapidly growing laboratory strain, our choice of *M. smegmatis* as a surrogate of *M. tuberculosis* was justified by an observed tendency of *Msm* to display drug susceptibility profile closer to MDR than drug-sensitive *M. tuberculosis* [32] and by the conservation of NAD target pathway and key enzymes therein. *Mt*NadD and *Ms*NadD bear high degree of sequence identity (75%), rising to nearly 100% in the conserved regions of active site (Supplementary Figure 1).

N2 inhibitors display on-target killing activity in replicative and nonreplicative conditions.

Despite encouraging low micromolar IC_{50} values, the N1 series resulted in poor *M. smegmatis* growth suppression (Table 1). At fixed concentration of 50 μM, the original N1 hit had no effect, while other N1 analogs produced at most a 50% growth suppression (Table 1). Moreover, the growth inhibition, when present, did not correlate with *Mt*NadD inhibition, pointing to possible off-target effects of this series of compounds. Indeed, class

N1 compounds are moderate to potent inhibitors of *M. tuberculosis* H37Rv fructose 1,6-biphosphate aldolase (FBA) as reported in PubChem Bioassay AID 588726. For instance, at 1 μM, primary hit **N1–13** and analog **N1–10** exert 40% and 20% inhibition of *Mt*FBA activity, respectively, with prospective IC_{50} values in the very low micromolar range. *Mt*FBA has been proposed as a new pharmacological target of *M. tuberculosis* since it is upregulated in latent TB[33]. Although an antibacterial molecule with dual-targeting mechanism presents obvious benefits such as, for instance, an expected low emergence of spontaneous resistance[34], the poor bioactivity in *M. smegmatis* led us to discard the N1 series for further characterization.

As opposed to N1 series, the N2 series of inhibitors display strong bactericidal activity against model *M. smegmatis* with MIC in the low micromolar range (Figure 3A–D and Table 2). Next, we reconfirmed a comparable bactericidal activity on *M. tuberculosis*, also for a few analogs that were not originally included in the previous HTS whole-cell bioassay (Table 2). For the most potent ones, we additionally measured MIC for *Mycobacterium abscessus*, a more divergent nontuberculous mycobacterium [35] with a conserved NAD target pathway. The strong growth suppression of *M. tuberculosis* and *M. smegmatis*, and the less pronounced inhibition of *M. abscessus*, demonstrates N2 inhibitors' specific targeting of NadD family in mycobacteria, and, in general, points to a protein target site potentially resilient to mutations. Furthermore, **N2–7** and **N2–11** caused rapid depletion of the NAD pool (Figure 3D, E), comparable to the effect of NadD "protein knockdown" as observed in our previous work[17], corroborating their on-target activity.

Using a carbon starvation model for the non-replicating state in *M. smegmatis*[17, 36], we observed a bactericidal effect even for dormant mycobacteria (Figure 3F). Up to 4 logs in colony forming unit (CFU) reduction was observed upon 96 h incubation with inhibitor **N2–11** (at 5× MIC dose), with almost no CFU reduction in parallel samples incubated with DMSO, linezolid (also at 5× MIC). The **N2–8** analog shows a more delayed, but substantial, effect with over 2 logs CFU decrease. Taken together, these results provide strong evidence that proposed inhibitors of series N2 are effective against replicative as well as non-replicative mycobacteria.

N2–11 inhibitor suppresses drug-resistant *Mtb*.

Having demonstrated that *Mt*NadD inhibitors suppress the growth of drug-tolerant mycobacteria, we next determined their activity on a panel of drug-resistant *Mtb* clinical isolates using a single dose assay in liquid media. We measured the effect of **N2–11** (at a concentration of 25 μM, 6-fold the MIC for *Mtb*) on two *Mtb* ATCC strains (H37Rv and PZA monoresistant), and four clinical drug-resistant isolates: pyrazinamide resistant (PZA-R), MDR, XDR, and totally drug-resistant (TDR). Growth controls were run in parallel in the presence and absence of DMSO. The results (Supplementary Figure 2) showed that the inhibitor halted completely the growth of all clinical isolates. Despite being a single-dose assay, these data establish that class N2 of *Mt*NadD inhibitors are promising to tackle drug-resistant tuberculosis.

Overexpression of NadD increases resistance to N2 series of inhibitors.

Overexpressing a gene encoding a drug target is expected to confer an increased resistance to that drug. Therefore, to genetically validate NadD as the molecular target of N2 inhibitors, we overexpressed *Mt*NadD in *M. smegmatis* using a nonintegrative pVV16-derived plasmid (see the Methods section for cloning details). To this aim, we generated two different versions of *Mt*NadD, wild-type NadD ($NadD_{WT}$) and $NadD_{\Delta 24}$, a non-functional version here used as a control [17]. In the presence of selected N2 inhibitors, the $NadD_{WT}$ strain consistently exhibited a larger MIC compared to $NadD_{\Delta 24}$ (~2-fold, Supplementary Figure 3). In addition, we included **N3–1**, a representative of the N3 series that we discarded earlier for its off-target mode of action. Coherently, with **N3–1** no MIC shift was observed between $NadD_{WT}$ and $NadD_{\Delta 24}$. Altogether, these data suggest that *Mt*NadD may indeed represent a specific molecular target of the N2 series, antimycobacterial molecules identified in this study.

Structure of *Mt*NadD in complex with inhibitor N2–8.

To elucidate the mechanism of *Mt*NadD inhibition by N2 class of inhibitors, rationalize the observed SAR, and guide future rational inhibitor design, we determined 1.86 Å resolution crystal structure in complex with inhibitor **N2–8**.

The structure was refined to R_{work} of 0.172 and R_{free} of 0.192 with excellent overall geometry (Table 4). There are two molecules of *Mt*NadD in the asymmetric unit (chain B and A in Figure 4A and Supplementary Figure 4A) that correspond to previously observed dimer in apo-structures of *Mt*NadD [26]. Two *Mt*NadD monomers have very similar structures with root mean square deviations (rmsd) of 1.2 Å over 186 Cα atoms (Supplementary Figure 4B). Analysis of the crystal contacts revealed the formation of dimer-of-dimers of *Mt*NadD (Figure 4A). This new quaternary structure was induced by the N2–8 ligand binding, with two molecules of the ligand bridging the dimers together. The crystallographically identical ligand binding sites are formed by chains B and A', and chains B' and A, respectively. Analysis by the PISA server classifies the interface between two *Mt*NadD dimers as stable. The clear electron density corresponding to inhibitor N2–8 allowed unambiguous modeling of the ligand (Figure 4 and Supplementary Figure 5). The inhibitor occupies a hydrophobic pocket formed by helices α5 and α6 of chain B and by helix a6 and strand b6 of chain A' (Figure 4B). Overall, **N2–8** exhibits high steric complementarity with the surface of the two *Mt*NadD chains. The menthol moiety of the inhibitor makes van der Waals contacts with several hydrophobic residues of the pocket (Figure 4B and Supplementary Figure 6). Additional contacts include residues L151 and L158 from chain A'.

Moreover, residue Glu160 contributes to the positioning of the positively charged benzimidazole core. The electron density for the phenoxymethyl part of the inhibitor is relatively poor compared with the rest of the inhibitor. The phenoxymethyl moiety could adopt multiple conformations, as it is oriented away from the protein. This is consistent with the SAR data on the N2 series of inhibitors that show that various sub-structures are permissible at R2 position (Figure 2 and Table 2). The inhibitor-binding site is located next to the active site of the enzyme (Figure 4C). The inhibitor-bound structure of *Mt*NadD•N2–8 is similar to our apo-structures of *Mt*NadD (PDB ID 4X0E and 4RPI) [26] with rmsd of 1.1–

1.6 Å over 177–188 Cα atoms (Figure 4C). This conformation represents an inactive state of the enzyme with a constricted active site that prevents the binding of both NaMN and ATP substrates. Here, helix α5 is displaced towards the active site in *Mt*NadD•N2–8 as well as in apo-structures of *Mt*NadD, compared to the structures of NadD bacterial homologs in product-bound state (Figure 4C). In particular, Ile114 lies in a clashing position with the nicotinic acid moiety of modeled NaAD. Additionally, Trp117 which should coordinate the nicotinic acid moiety of NaMN or NaAD is rotated outside of the active site. Moreover, Leu164, a key residue in ATP substrate recognition and stabilization [26], is similarly oriented as in the apo-form and blocks the access of the ATP substrate (Figure 4C).

Besides freezing the enzyme in a non-productive conformation, the **N2–8** inhibitor plays an active role in the active site destabilization. Most prominently, the side chain of Asp109 is flipped away from the active site towards to the inhibitor due to the electrostatic interaction with the positive charge on the benzimidazole ring (at a distance of about 4 Å) (Figure 4B, C). Asp109 is a strictly conserved residue for the entire NaMN/NMN-AT family [26] which forms an H-bond with the 2'-OH of the AMP ribose[37] and is thought to help with essential Mg^{+2} coordination during catalysis[38]. Its essentiality has been recently demonstrated by site-directed mutagenesis in *Plasmodium falciparum* NMN-AT [39]. Finally, two salt bridges Asp29-Lys47 further stabilize the two dimers of this inhibitor-driven quaternary structure (Supplementary Figure 7). Notably, Lys47 is part of the PPH(K/R) loop motif involved in the recognition of NaMN phosphate, and found to be essential for catalysis in our previous study [26]. Thus, the newly formed electrostatic interaction may seize Lys47 in a nonfunctional state.

DISCUSSION

Over the past years, conventional target-directed drug discovery has not met expectations, with an increasing spending accompanied by less delivery of new drugs to the market [40]. Among well-known drawbacks of target-based strategies for antibacterial development are rapid evolution of resistance of single targets, the difficulty of developing broad-spectrum compounds, and the lack of whole cell activity of many potent biochemical hits. With respect to TB, the high resistance frequency of a single-target agent is less important, since combination drug therapy is always employed. Narrow-spectrum agents that do not affect the commensal microbiota would be also particularly valuable, since the lengthy treatment regimens required for the treatment of TB and MDR-TB have detrimental effect upon the host microbiome. Thus, a novel, target-based screen of potent hits resulted from phenotypic screen could be a promising strategy to develop smarter antitubercular drugs. NAD biosynthesis represents a validated pathway in *Mtb* and other bacterial pathogens for antibiotic development.

Here, we describe the identification and initial SAR analysis of *Mt*NadD inhibitors with potent antimycobacterial activity through an initial target-based screen of whole cell active compounds. This approach yielded compounds that were 5-fold more potent against the purified enzyme and over 10-fold more effective against model *M. smegmatis* than those reported in our initial effort [26].

These compounds maintain strong bactericidal effect against *M. tuberculosis* and some clinical isolates of MDR-, XDR-, and TDR-*Mtb* as well as a prominent bactericidal effect under non-replicating conditions in *M. smegmatis*. This represents the first evidence that pharmacological inhibition of *Mt*NadD and, potentially, other essential NAD-related enzymes, is a valuable strategy to kill dormant and resistant *Mtb* strains which could be exploited alone or in combination with other drugs, e.g. targeting energy metabolism.

In our previous study, we proposed that in dormant cells *Mt*NadD target is in a closed, inactive conformation. A shift into a catalytically active conformation would be induced by the increased ATP substrate levels reflecting the high respiratory activity of actively replicating cells. *Mt*NadD enzymatic dormancy hinted for a previously unexplored strategy for development of small molecule inhibitors that would target and further stabilize the catalytically inactive closed form of the enzyme. Here, we report a crystal structure of *Mt*NadD in complex with the benzimidazolium salt derivative **N2–8** that locks the enzyme in a nonproductive conformation, thus setting the stage for future lead optimization efforts. The 3D analysis revealed that the inhibitor surprisingly interacts with a largely hydrophobic pocket at the dimer interface of ligand-induced, dimer-of-dimers quaternary structure. The fact that small molecule binding could involve new or perturbed quaternary structure is not unprecedented. Indeed, several studies, including our own work with a NadD homolog described the formation of a new dimeric assembly upon binding of inhibitor [25, 41].

Various anti-mycobacterial compounds incorporate the benzimidazole substructure [42]. We provided unequivocal evidence that N2 series of *Mt*NadD inhibitors act on target by detecting (i) a 2-fold increase of MIC in a Mycobacterium strain overexpressing *Mt*NadD and (ii) a rapid decline of the pathway end-product NAD. Furthermore, close inspection of the chemistry of N2 series of inhibitors reveals their uniqueness and novelty. Firstly, they have substitutions at both N atoms of benzimidazole core that are not tolerated for an anti-TB activity, as recently reviewed [42]. By virtue of these substitutions, the compounds are positively charged benzimidazolium ions, as opposed to neutral anti-TB benzimidazole derivatives reported so far. The net positive charge of the benzimidazolium core is indeed critical for the inhibition of *Mt*NadD target enzyme as it perturbs the essential Asp109 catalytic site residue and helps bridging the dimers of the induced quaternary structure by interacting with Glu160. Secondly, N2 inhibitors feature a bulky menthol acetate substituent which engages most contacts with the protein. Moreover, through a cheminformatics survey in the PubChem databases we identified analogs of some N2 inhibitors that lack the menthol acetate moiety, resulting in neutral benzimidazoles. Strikingly, such compounds were screened in as many as three independent *M. tuberculosis* whole-cell bioassays, and all resulted to be inactive (Supplementary Table 2).

Our study introduces a strategy for inhibiting the essential bacterial NaMN adenylyltransferase that targets a unique, unexplored pocket, independent from the active site. Previous screening campaigns have concentrated their efforts on targeting the enzyme active site or sub-sites, with modest outcomes. Indeed, this enzyme family features a large active site with an ATP binding pocket, and its targeting may lead to extensive cross-reactivity with nucleotide binding pockets on several different proteins. Thus, our approach targeting a unique novel pocket represents a significant step forward that can circumvent

the abovementioned limitations. Future extensions of this work will include improvement of chemical activity of the lead compounds by further exploring chemical diversity space to bring them into a viable therapeutic range as potential stand-alone drugs or in combination with other TB drugs.

In conclusion, this study demonstrates the successful application of combined target-directed and phenotypic screen to arrive at novel scaffolds inhibiting mycobacterial NadD. Among the three identified scaffolds, the most promising one, containing a benzimidazolium core substituted with a menthol acetate group, has been characterized in detail revealing its potential for chemical optimization. Different analogs have shown to inhibit the growth of several Mycobacteria, including drug resistant *M. tuberculosis*, dormant *M. smegmatis,* and the pathogenic *M. abscessus*. These molecules inhibit the protein by displaying a novel mechanism and by binding to a unique site on the enzyme.

METHODS

Details of experimental procedures are provided in Supporting Information.

Supplementary Material

Refer to Web version on PubMed Central for supplementary material.

ACKNOWLEDGMENTS

We thank the Global Alliance for TB Drug Development (TB Alliance) for providing the TB whole cell active compounds library (TBAC). We are grateful to Eric Rubin (Harvard Medical School) for consultations on mycobacterial physiology and drug discovery. We would like to thank Lauren Brumsey for constructing *Mt*NadD overexpressing *M. smegmatis* strains. We thank the staff members of Southeast Regional Collaborative Access Team (SER-CAT) at the Advanced Photon Source, Argonne National Laboratory, for assistance during data collection. Use of the Advanced Photon Source was supported by the U. S. Department of Energy, Office of Science, Office of Basic Energy Sciences, under Contract No. W-31–109-Eng-38. Research reported in this publication was partially supported by the National Institute of Allergy and Infectious Diseases grant number R03AI117361 to KVK, Montalcini International Program 2009 and Grant RSA2013–14 through the Italian Ministry of Education, Universities and Research to LS, and the Lead Generation Initiative to AO and E.S at SBP.

REFERENCES

[1]. WHO. (2017) Global tuberculosis report.

[2]. Fattorini L, Piccaro G, Mustazzolu A, and Giannoni F (2013) Targeting dormant bacilli to fight tuberculosis, Mediterr J Hematol Infect Dis 5, e2013072. [PubMed: 24363887]

[3]. Gengenbacher M, and Kaufmann SH (2012) Mycobacterium tuberculosis: success through dormancy, FEMS Microbiol Rev 36, 514–532. [PubMed: 22320122]

[4]. Rohde K, Yates RM, Purdy GE, and Russell DG (2007) Mycobacterium tuberculosis and the environment within the phagosome, Immunol Rev 219, 37–54. [PubMed: 17850480]

[5]. Trauner A, Borrell S, Reither K, and Gagneux S (2014) Evolution of drug resistance in tuberculosis: recent progress and implications for diagnosis and therapy, Drugs 74, 1063–1072. [PubMed: 24962424]

[6]. Gandhi NR, Nunn P, Dheda K, Schaaf HS, Zignol M, van Soolingen D, Jensen P, and Bayona J (2010) Multidrug-resistant and extensively drug-resistant tuberculosis: a threat to global control of tuberculosis, Lancet 375, 1830–1843. [PubMed: 20488523]

[7]. Andries K, Verhasselt P, Guillemont J, Gohlmann HW, Neefs JM, Winkler H, Van Gestel J, Timmerman P, Zhu M, Lee E, Williams P, de Chaffoy D, Huitric E, Hoffner S, Cambau E,

Truffot-Pernot C, Lounis N, and Jarlier V (2005) A diarylquinoline drug active on the ATP synthase of Mycobacterium tuberculosis, Science 307, 223–227. [PubMed: 15591164]

[8]. Koul A, Dendouga N, Vergauwen K, Molenberghs B, Vranckx L, Willebrords R, Ristic Z, Lill H, Dorange I, Guillemont J, Bald D, and Andries K (2007) Diarylquinolines target subunit c of mycobacterial ATP synthase, Nat Chem Biol 3, 323–324. [PubMed: 17496888]

[9]. Chen X, Hashizume H, Tomishige T, Nakamura I, Matsuba M, Fujiwara M, Kitamoto R, Hanaki E, Ohba Y, and Matsumoto M (2017) Delamanid Kills Dormant Mycobacteria In Vitro and in a Guinea Pig Model of Tuberculosis, Antimicrob Agents Chemother 61.

[10]. Xavier AS, and Lakshmanan M (2014) Delamanid: A new armor in combating drug-resistant tuberculosis, J Pharmacol Pharmacother 5, 222–224. [PubMed: 25210407]

[11]. Cook GM, Hards K, Dunn E, Heikal A, Nakatani Y, Greening C, Crick DC, Fontes FL, Pethe K, Hasenoehrl E, and Berney M (2017) Oxidative Phosphorylation as a Target Space for Tuberculosis: Success, Caution, and Future Directions, Microbiol Spectr 5.

[12]. Huitric E, Verhasselt P, Koul A, Andries K, Hoffner S, and Andersson DI (2010) Rates and mechanisms of resistance development in Mycobacterium tuberculosis to a novel diarylquinoline ATP synthase inhibitor, Antimicrob Agents Chemother 54, 1022–1028. [PubMed: 20038615]

[13]. Koul A, Vranckx L, Dhar N, Gohlmann HW, Ozdemir E, Neefs JM, Schulz M, Lu P, Mortz E, McKinney JD, Andries K, and Bald D (2014) Delayed bactericidal response of Mycobacterium tuberculosis to bedaquiline involves remodelling of bacterial metabolism, Nat Commun 5, 3369. [PubMed: 24569628]

[14]. Boshoff HI, Xu X, Tahlan K, Dowd CS, Pethe K, Camacho LR, Park TH, Yun CS, Schnappinger D, Ehrt S, Williams KJ, and Barry CE 3rd. (2008) Biosynthesis and recycling of nicotinamide cofactors in mycobacterium tuberculosis. An essential role for NAD in nonreplicating bacilli, J Biol Chem 283, 19329–19341. [PubMed: 18490451]

[15]. Vilcheze C, Weinrick B, Wong KW, Chen B, and Jacobs WR Jr. (2010) NAD+ auxotrophy is bacteriocidal for the tubercle bacilli, Mol Microbiol 76, 365–377. [PubMed: 20199601]

[16]. Ying W, Chen Y, Alano CC, and Swanson RA (2002) Tricarboxylic acid cycle substrates prevent PARP-mediated death of neurons and astrocytes, J Cereb Blood Flow Metab 22, 774–779. [PubMed: 12142562]

[17]. Rodionova IA, Schuster BM, Guinn KM, Sorci L, Scott DA, Li X, Kheterpal I, Shoen C, Cynamon M, Locher C, Rubin EJ, and Osterman AL (2014) Metabolic and bactericidal effects of targeted suppression of NadD and NadE enzymes in mycobacteria, MBio 5, e00747–00713. [PubMed: 24549842]

[18]. Kim JH, O'Brien KM, Sharma R, Boshoff HI, Rehren G, Chakraborty S, Wallach JB, Monteleone M, Wilson DJ, Aldrich CC, Barry CE 3rd, Rhee KY, Ehrt S, and Schnappinger D (2013) A genetic strategy to identify targets for the development of drugs that prevent bacterial persistence, Proc Natl Acad Sci U S A 110, 19095–19100. [PubMed: 24191058]

[19]. Gerdes SY, Scholle MD, D'Souza M, Bernal A, Baev MV, Farrell M, Kurnasov OV, Daugherty MD, Mseeh F, Polanuyer BM, Campbell JW, Anantha S, Shatalin KY, Chowdhury SA, Fonstein MY, and Osterman AL (2002) From genetic footprinting to antimicrobial drug targets: examples in cofactor biosynthetic pathways, J Bacteriol 184, 4555–4572. [PubMed: 12142426]

[20]. Osterman AL, and Begley TP (2007) A subsystems-based approach to the identification of drug targets in bacterial pathogens, *Progress in drug research*. Fortschritte der Arzneimittelforschung. Progres des recherches pharmaceutiques 64, 131, 133–170.

[21]. Sorci L, Blaby I, De Ingeniis J, Gerdes S, Raffaelli N, de Crecy Lagard V, and Osterman A (2010) Genomics-driven reconstruction of acinetobacter NAD metabolism: insights for antibacterial target selection, J Biol Chem 285, 39490–39499. [PubMed: 20926389]

[22]. Sorci L, Blaby IK, Rodionova IA, De Ingeniis J, Tkachenko S, de Crecy-Lagard V, and Osterman AL (2013) Quinolinate salvage and insights for targeting NAD biosynthesis in group A streptococci, J Bacteriol 195, 726–732. [PubMed: 23204464]

[23]. Sorci L, Kurnasov O, Rodionov DA, and Osterman AL (2010) Genomics and Enzymology of NAD Biosynthesis, In Comprehensive Natural Products II (Lew M, and Hung-Wen L, Eds.), pp 213–257, Elsevier, Oxford.

[24]. Sorci L, Pan Y, Eyobo Y, Rodionova I, Huang N, Kurnasov O, Zhong S, MacKerell AD Jr., Zhang H, and Osterman AL (2009) Targeting NAD biosynthesis in bacterial pathogens: Structure-based development of inhibitors of nicotinate mononucleotide adenylyltransferase NadD, Chemistry & biology 16, 849–861. [PubMed: 19716475]

[25]. Huang N, Kolhatkar R, Eyobo Y, Sorci L, Rodionova I, Osterman AL, Mackerell AD, and Zhang H (2010) Complexes of bacterial nicotinate mononucleotide adenylyltransferase with inhibitors: implication for structure-based drug design and improvement, J Med Chem 53, 5229–5239. [PubMed: 20578699]

[26]. Rodionova IA, Zuccola HJ, Sorci L, Aleshin AE, Kazanov MD, Ma CT, Sergienko E, Rubin EJ, Locher CP, and Osterman AL (2015) Mycobacterial nicotinate mononucleotide adenylyltransferase: structure, mechanism, and implications for drug discovery, J Biol Chem 290, 7693–7706. [PubMed: 25631047]

[27]. Orsomando G, Agostinelli S, Bramucci M, Cappellacci L, Damiano S, Lupidi G, Maggi F, Kamte SLN, Nya PCB, Papa F, Petrelli D, Quassinti L, Sorci L, Vitali LA, and Petrelli R (2016) Mexican sunflower (Tithonia diversifolia, Asteraceae) volatile oil as a selective inhibitor of Staphylococcus aureus nicotinate mononucleotide adenylyltransferase (NadD), Ind Crop Prod 85, 181–189.

[28]. Moro WB, Yang Z, Kane TA, Brouillette CG, and Brouillette WJ (2009) Virtual screening to identify lead inhibitors for bacterial NAD synthetase (NADs), Bioorg Med Chem Lett 19, 2001–2005. [PubMed: 19249205]

[29]. Petrelli R, Sham YY, Chen L, Felczak K, Bennett E, Wilson D, Aldrich C, Yu JS, Cappellacci L, Franchetti P, Grifantini M, Mazzola F, Di Stefano M, Magni G, and Pankiewicz KW (2009) Selective inhibition of nicotinamide adenine dinucleotide kinases by dinucleoside disulfide mimics of nicotinamide adenine dinucleotide analogues, Bioorg Med Chem 17, 5656–5664. [PubMed: 19596199]

[30]. Ananthan S, Faaleolea ER, Goldman RC, Hobrath JV, Kwong CD, Laughon BE, Maddry JA, Mehta A, Rasmussen L, Reynolds RC, Secrist JA 3rd, Shindo N, Showe DN, Sosa MI, Suling WJ, and White EL (2009) High-throughput screening for inhibitors of Mycobacterium tuberculosis H37Rv, Tuberculosis (Edinb) 89, 334–353. [PubMed: 19758845]

[31]. Maddry JA, Ananthan S, Goldman RC, Hobrath JV, Kwong CD, Maddox C, Rasmussen L, Reynolds RC, Secrist JA 3rd, Sosa MI, White EL, and Zhang W (2009) Antituberculosis activity of the molecular libraries screening center network library, Tuberculosis (Edinb) 89, 354–363. [PubMed: 19783214]

[32]. Chaturvedi V, Dwivedi N, Tripathi RP, and Sinha S (2007) Evaluation of Mycobacterium smegmatis as a possible surrogate screen for selecting molecules active against multi-drug resistant Mycobacterium tuberculosis, J Gen Appl Microbiol 53, 333–337. [PubMed: 18187888]

[33]. de la Paz Santangelo M, Gest PM, Guerin ME, Coincon M, Pham H, Ryan G, Puckett SE, Spencer JS, Gonzalez-Juarrero M, Daher R, Lenaerts AJ, Schnappinger D, Therisod M, Ehrt S, Sygusch J, and Jackson M (2011) Glycolytic and non-glycolytic functions of Mycobacterium tuberculosis fructose-1,6-bisphosphate aldolase, an essential enzyme produced by replicating and non-replicating bacilli, J Biol Chem 286, 40219–40231. [PubMed: 21949126]

[34]. Mani N, Gross CH, Parsons JD, Hanzelka B, Muh U, Mullin S, Liao Y, Grillot AL, Stamos D, Charifson PS, and Grossman TH (2006) In vitro characterization of the antibacterial spectrum of novel bacterial type II topoisomerase inhibitors of the aminobenzimidazole class, Antimicrob Agents Chemother 50, 1228–1237. [PubMed: 16569833]

[35]. Lee MR, Sheng WH, Hung CC, Yu CJ, Lee LN, and Hsueh PR (2015) Mycobacterium abscessus Complex Infections in Humans, Emerg Infect Dis 21, 1638–1646. [PubMed: 26295364]

[36]. Singla D, Tewari R, Kumar A, Raghava GP, and Open Source Drug Discovery, C. (2013) Designing of inhibitors against drug tolerant Mycobacterium tuberculosis (H37Rv), Chem Cent J 7, 49. [PubMed: 23497593]

[37]. Zhang H, Zhou T, Kurnasov O, Cheek S, Grishin NV, and Osterman A (2002) Crystal structures of E. coli nicotinate mononucleotide adenylyltransferase and its complex with deamido-NAD, Structure 10, 69–79. [PubMed: 11796112]

[38]. D'Angelo I, Raffaelli N, Dabusti V, Lorenzi T, Magni G, and Rizzi M (2000) Structure of nicotinamide mononucleotide adenylyltransferase: a key enzyme in NAD(+) biosynthesis, Structure 8, 993–1004. [PubMed: 10986466]

[39]. O'Hara JK, Kerwin LJ, Cobbold SA, Tai J, Bedell TA, Reider PJ, and Llinas M (2014) Targeting NAD+ metabolism in the human malaria parasite Plasmodium falciparum, PLoS One 9, e94061. [PubMed: 24747974]

[40]. Silver LL (2011) Challenges of antibacterial discovery, Clin Microbiol Rev 24, 71–109. [PubMed: 21233508]

[41]. Thangavelu K, Pan CQ, Karlberg T, Balaji G, Uttamchandani M, Suresh V, Schuler H, Low BC, and Sivaraman J (2012) Structural basis for the allosteric inhibitory mechanism of human kidney-type glutaminase (KGA) and its regulation by Raf-Mek-Erk signaling in cancer cell metabolism, Proc Natl Acad Sci U S A 109, 7705–7710. [PubMed: 22538822]

[42]. Keri RS, Rajappa CK, Patil SA, and Nagaraja BM (2016) Benzimidazole-core as an antimycobacterial agent, Pharmacol Rep 68, 1254–1265. [PubMed: 27686965]

[43]. Karplus PA, and Diederichs K (2012) Linking crystallographic model and data quality, Science 336, 1030–1033. [PubMed: 22628654]

[44]. Kabsch W (2010) Xds, Acta Crystallogr D Biol Crystallogr 66, 125–132. [PubMed: 20124692]

[45]. Chen VB, Arendall WB 3rd, Headd JJ, Keedy DA, Immormino RM, Kapral GJ, Murray LW, Richardson JS, and Richardson DC (2010) MolProbity: all-atom structure validation for macromolecular crystallography, Acta Crystallogr D Biol Crystallogr 66, 12–21. [PubMed: 20057044]

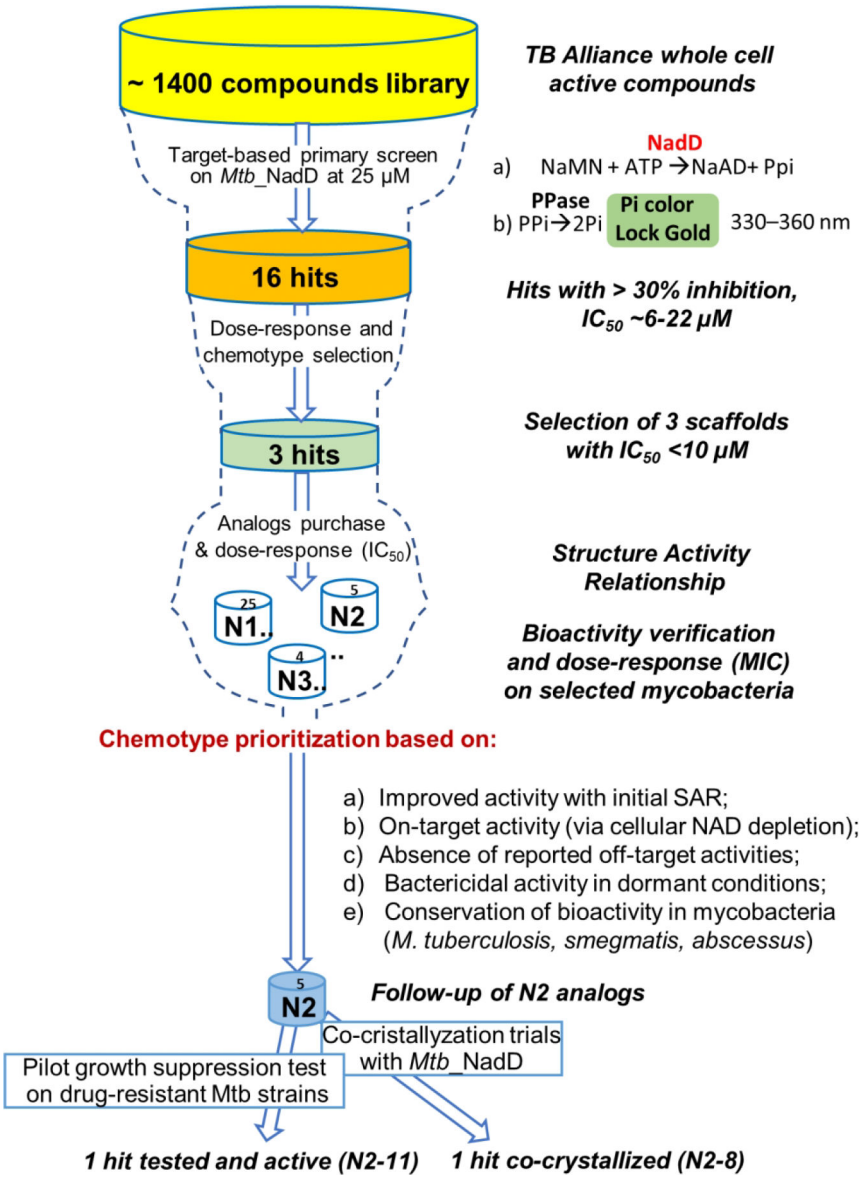

Figure 1. Flowchart of the whole-cell and target screening approach for delivering novel antitubercular NaMN adenylyltransferase inhibitors.

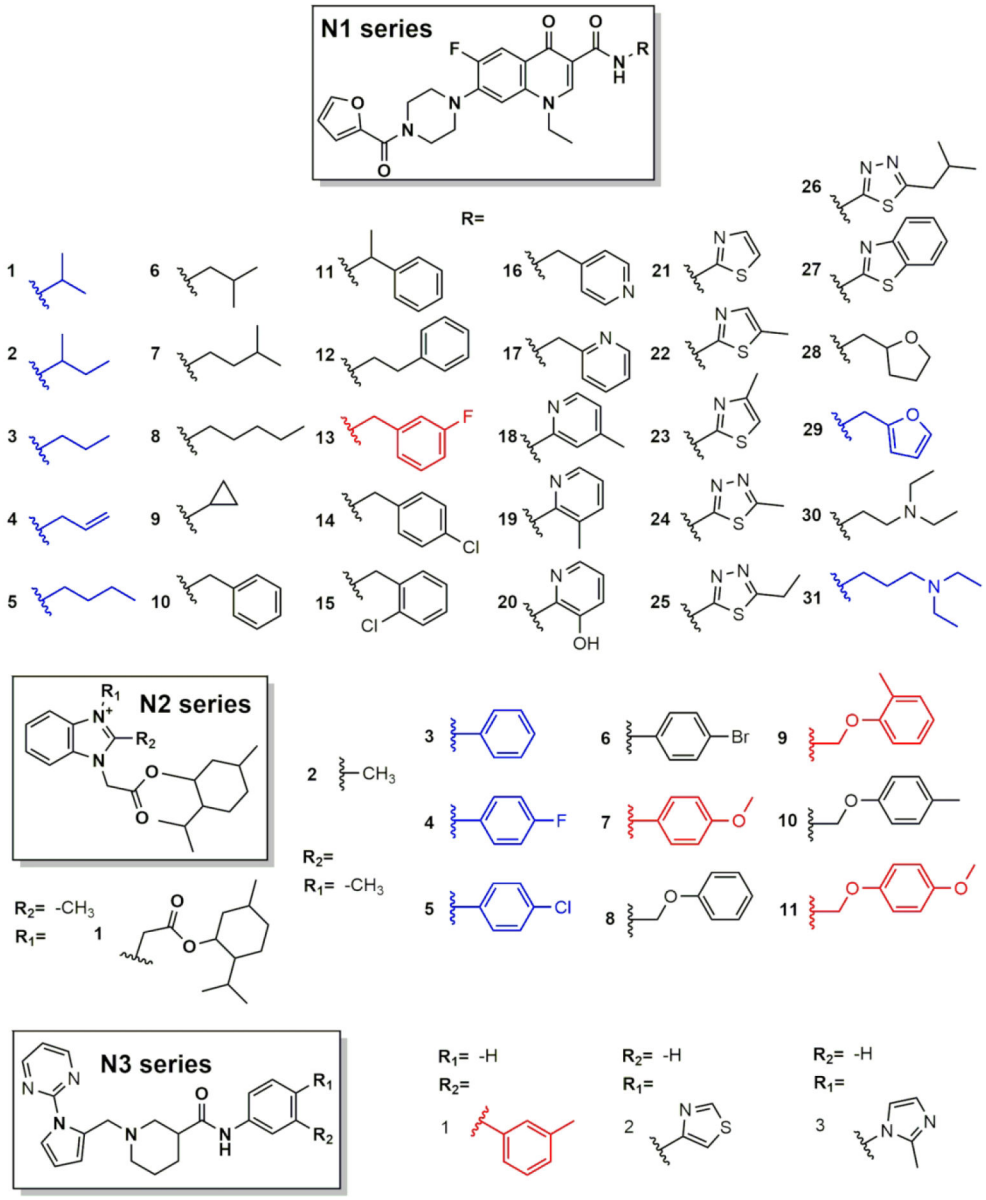

Figure 2. Chemical diversity of the 3 series of novel *Mt*NadD inhibitors evaluated.

In red, molecules that were identified in our primary screen of the TB Alliance bioactive library against *Mt*NadD (IC_{50} < 20 μM). In black, novel analogues for each chemotype tested in this study. In blue, analogs that were not tested in our study, but for which a relevant activity against *M. tuberculosis* or a *Mtb* target enzyme has been reported in PubChem (see Tables 1–2 and main text for details).

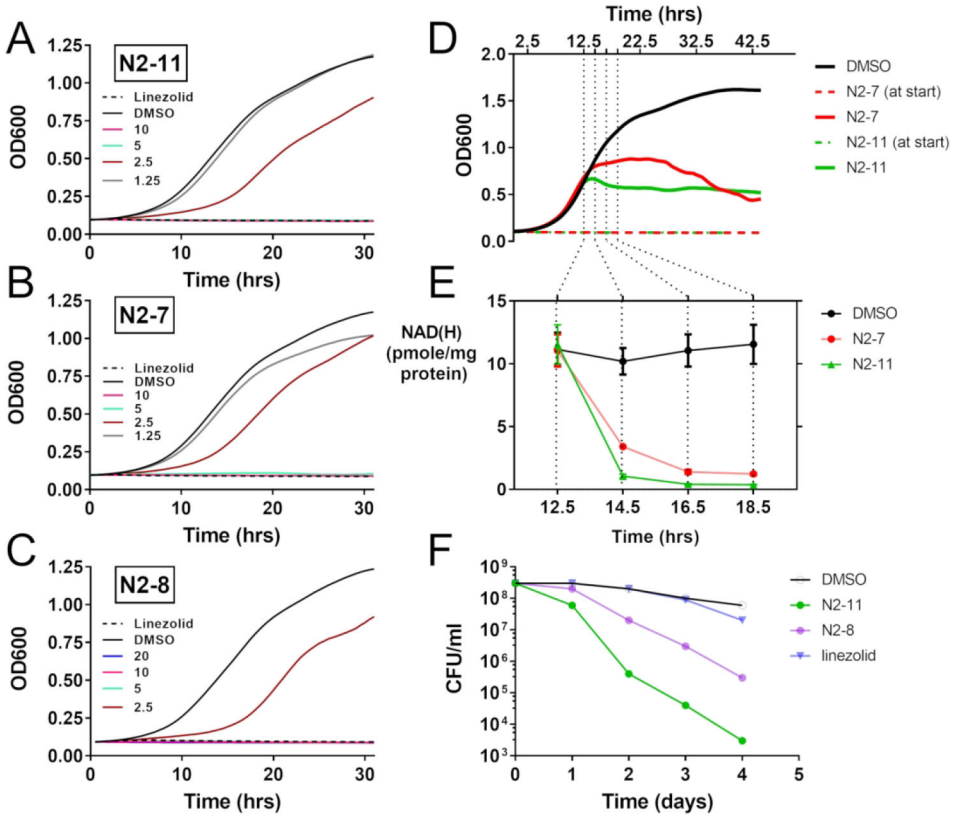

Figure 3. Bactericidal, on-target effects of N2 inhibitors in replicating and non-replicating *M. smegmatis*.

(A-C) Growth suppression curves at different N2 series inhibitors' concentrations underline their killing activity on replicating *Msm* at above 5 μM. DMSO at 1 % represents the "no inhibitor" control. Linezolid at 3 μM was used as a positive control. (D) Addition of the inhibitor at ~5× MIC concentration at log-phase (after 12.5 hours of growth) stops the growth of *Msm* and (E) rapidly deplete NAD pool. Residual levels of NAD were measured by a colorimetric detection kit and normalized by total protein in samples taken for 6 hours, in 2 hours' time interval. (F) Cell viability by CFU assay after 1–4 days of incubation of *Msm* with 5xMIC inhibitor (25 μM) under carbon starvation conditions. In this case, Linezolid was used at 15 μM.

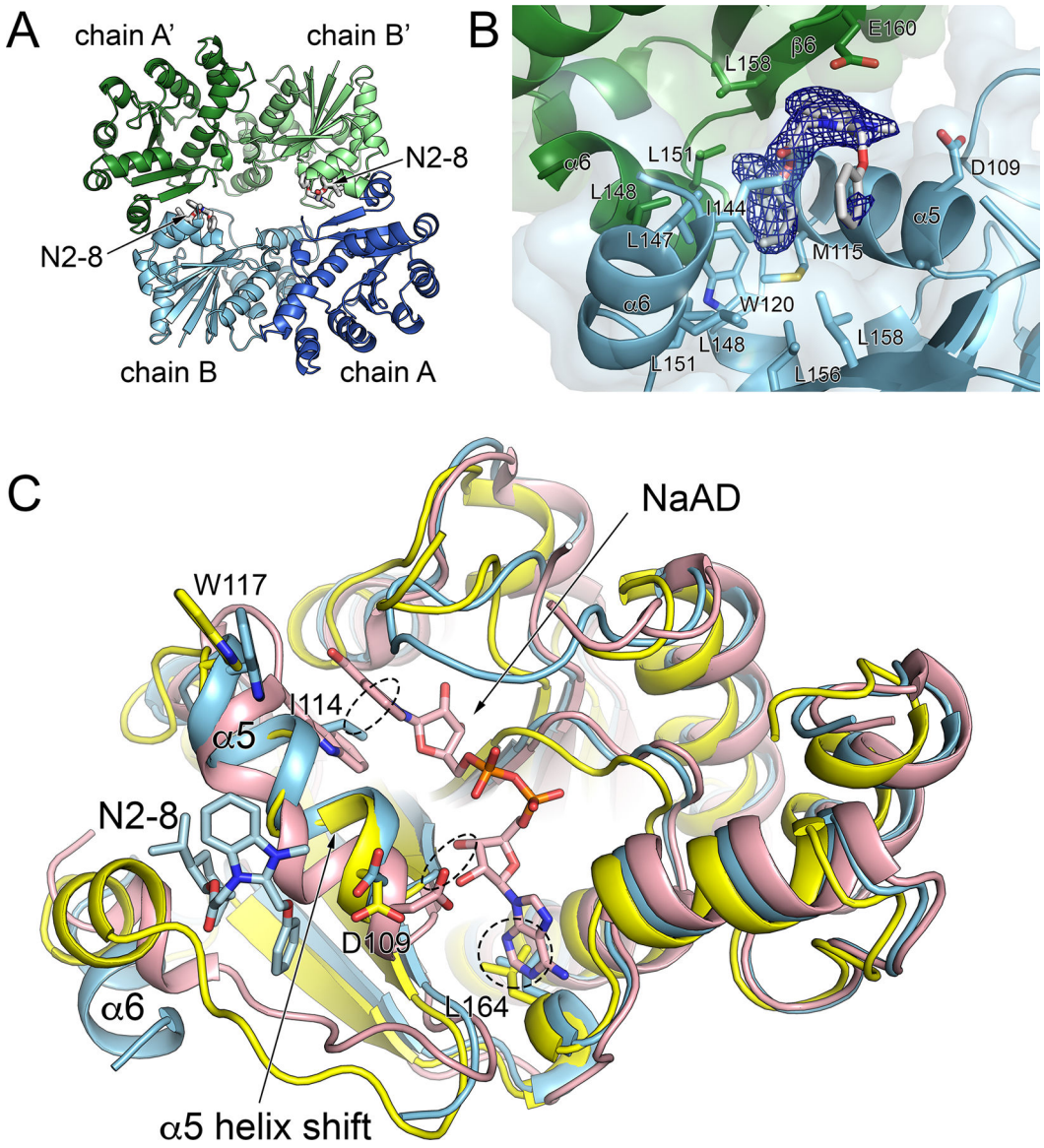

Figure 4. Structure of *Mt*NadD in complex with inhibitor N2–8.

(A) Two **N2–8** binding pockets induce the formation of dimer-of-dimers of *Mt*NadD. The asymmetric unit dimer A-B is shown in shades of blue; the crystallographic symmetry dimer A'-B' is shown in shades of green. (B) A close-up view of the **N2–8** binding site. The hydrophobic residues lining up the inhibitor binding site are shown in sticks representation. σA-weighted $2F_O–F_C$ electron density map contoured at 1σ is shown as blue mesh. (C) Comparison of the closed active-site conformation of *Mt*NadD•**N2–8** complex (light blue) with *Mt*NadD apo structure (yellow) (PDB ID, 4X0E) and *Ma*NadD•NaAD complex structure (purple) (PDB ID, 5DEO). H-bonding between D109 and the adenosine moiety of the *Ma*NadD•NaAD complex is shown as dashed line. The steric clashes of L164 with adenine ring, I113 with nicotinate ring, and G106 with the AMP ribose are marked by dotted circles.

Table 1.

Inhibitory properties of N1 class *Mt*NadD inhibitors

ID	PubChem CID	Enzyme inhibition		Mycobacterium Growth inhibition		
		IC_{50} (μM)	(%) at 1 μM	*(%)* at 50 μM	MIC (μM)	
					tuberculosis	
		*Mt*NadD[a]	*Mt*FBA[b]	*smegmatis*[c]	*d*	*e*
N1–1	1900457	–	54.81	–	–	>25
N1–2	3772903	–	54.28	–	–	50
N1–3	1898472	–	79.9	–	–	25
N1–4	1894659	–	97.0	–	–	25
N1–5	1898131	–	22.14	–	–	>25
N1–6	1119724	24.8±4	11.37	nd	–	nd
N1–7	3807641	17.4±3.4	14.68	nd	–	>25
N1–8	1896721	34.0±8.7	–	~50	–	–
N1–9	1896658	41.6±7.9	–	~20	–	–
N1–10	1203235	3.7±0.6	20.43	nd	<10	25
N1–11	3722630	2.5±0.3	–	~50	–	–
N1–12	3697907	29.6±6.2	–	nd	–	–
N1–13	1898213	13.3±2.9	38.2	nd	12.5	25
N1–14	1203236	14.3±2.2	–	nd	–	–
N1–15	1119726	5.3±1.8	–	nd	–	–
N1–16	1893392	76.1±16.4	41.76	~20	>100	nd
N1–17	1203237	>100	–	nd	–	–
N1–18	1899519	25.7±9.2	–	~50	–	–
N1–19	1896369	>50	–	~100	–	–
N1–20	1898247	97.8±47.8	14.6	~10	–	nd
N1–21	1122203	>100	–	~20	–	–
N1–22	1122208	>100	–	nd	–	–
N1–23	1122206	>50	–	nd	–	–
N1–24	1122209	>50	–	nd	–	–
N1–25	1898735	>50	–	nd	–	–
N1–26	1423254	>50	–	nd	–	–
N1–27	1897037	>100	–	nd	–	–
N1–28	3774654	>100	–	nd	–	–
N1–29	658395	–	19.8	–	>10	<25
N1–30	16682092	>100	22.17	~20	>100	nd
N1–31	3333039	–	54.21	–	–	>25

[a] Assays performed in duplicate in at least 5 different inhibitors concentration. Standard errors are reported.

[b] *In vitro* inhibition of *M. tuberculosis* H37Rv fructose-bisphosphate aldolase (FBA), as reported in PubChem Bioassay AID 588726.

[c] Antibacterial activity against *M. smegmatis* is expressed as percentage of growth suppression at fixed 50 μM concentration, except for **N1–18** that was tested at 20 μM.

[d] Values are deduced from PubChem Bioassay AID 1626 data.

[e] Values obtained from PubChem Bioassay AID 449762 data. "–", not assayed; nd, no detected effect. In red, compounds identified in the primary screening. In blue, analogs identified via cheminformatics search for which a bioactivity is reported, but not tested in our study.

Table 2.

Inhibitory properties of N2 class *Mt*NadD inhibitors evaluated

ID	PubChem CID	*Mt*NadD[a] IC_{50} (μM)	Mycobacterium Growth inhibition, MIC (μM)				
			smegmatis	*tuberculosis*			*abscessus*
					b	*c*	
N2–1	2834410	4.8±0.7	5	46.7	–	–	61.4
N2–2	2834412	111±16	25	–	–	–	–
N2–3	2834423	–	–	–	I	I	–
N2–4	2834427	–	–	–	32.7	28	–
N2–5	2834425	–	–	–	I	I	–
N2–6	2834414	45.5±15.8	25	–	I	I	–
N2–7	2834416	12.6±2.8	5	–	16.6	–	–
N2–8	2834419	17.9±2.2	5	21.2	I	I	26.7
N2–9	16192954	18.2±2.6	5	38.5	10.4	I	26.2
N2–10	3908383	19.5±2.5	5	19.7	–	–	25.6
N2–11	16195070	6.3±1.1	5	28.2	15.9	I	26

[a]Assays performed in duplicate in at least 5 different inhibitors concentration. Standard errors are reported. "–", not assayed; nd, no detected effect.

[b,c]Values deduced from PubChem Bioassay AID 1626 and AID 449762 data, respectively. For consistency, these values represent the minimal inhibitory concentration yielding >99% growth suppression and were obtained by fitting the reported EC_{50} and Hill Slope values into ECanything built-in equation in Prism 7.0. I, compounds tagged as "Inconclusive" and which showed >98% inhibition at a single concentration of 25 μM". No dose-response analysis was carried out. ID color- coding is as in Table 1.

Table 3.

Inhibitory properties of N3 class *Mt*NadD inhibitors[a]

ID	*Mt*NadD IC_{50} (μM)	Growth inhibition, MIC (μM)		
		M. smegmatis	*M. tuberculosis*	*M. abscessus*
N3–1	10.5±1.2	10	3.1	20.9
N3–2	96.4±25.9	>50	>100	>100
N3–3	>100	nd	–	–

[a]Assays performed in duplicate in at least 5 different inhibitors concentration. Standard errors are reported. "–", not assayed; nd, no detected effect (at 50 μM). ID color-coding is as in Tables 1 and 2.

Table 4.

Data collection and refinement statistics.

	M. tuberculosis **NadD in complex with N2–8 (PDB 6BUV)**
Data collection	
Wavelength (Å)	1.0000
Space group	*H*32
Cell dimensions:	
a, *b*, *c* (Å)	163.73, 163.73, 153.65
α, β, γ (°)	90, 90, 120
Resolution (Å)	52.1–1.86 (1.91–1.86)[a]
R_{sym}	0.077 (1.146)
$CC_{1/2}$[b]	99.6 (54.7)
$I / \sigma I$	11.08 (1.72)
Completeness (%)	99.3 (100.0)
Multiplicity	3.8 (3.8)
Refinement	
Resolution (Å)	52.1–1.86
No. reflections (total / free)	65711 / 5923
R_{work} / R_{free}	0.172 / 0.192
Number of atoms:	
Protein	2976
Ligand/ion	38
Water	296
B-factors:	
Protein	43.7
Ligand/ion	60.7
Water	49.6
All atoms	44.4
Wilson *B*	33.4
R.m.s. deviations:	
Bond lengths (Å)	0.008
Bond angles (°)	1.008
Ramachandran distribution[c] (%):	
Favored	98.9
Allowed	1.1
Outliers	0
Rotamer outliers[c] (%)	0
Clashscore[d]	2.53
MolProbity score[e]	1.04

[a]Values in parentheses are for the highest-resolution shell.

[b] $CC_{1/2}$ correlation coefficient as defined in Karplus & Diederichs [43] and calculated by *XSCALE* [44].

[c] Calculated using the MolProbity server (http://molprobity.biochem.duke.edu) [45].

[d] Clashscore is the number of serious steric overlaps (> 0.4 Å) per 1000 atoms.

[e] MolProbity score combines the clashscore, rotamer, and Ramachandran evaluations into a single score, normalized to be on the same scale as X-ray resolution [45].